Available online at www.sciencedirect.com
ScienceDirect
Trans. Nonferrous Met. Soc. China 34(2024) 3016−3028
Transactions of Nonferrous Metals Society of China
www.tnmsc.cn

Effect of inorganic salt impurities on seeded precipitation of silica hydrate from sodium silicate solution

Xiao-bin LI, Xiao-bing GAO, Qiu-sheng ZHOU, Yi-lin WANG, Tian-gui QI, Lei-ting SHEN, Gui-hua LIU, Zhi-hong PENG

School of Metallurgy and Environment, Central South University, Changsha 410083, China

Received 26 March 2023; accepted 8 October 2023

Abstract: To clarify the precipitation of silica hydrate from the real desilication solutions of aluminosilicate solid wastes by adding seeds and improve integrated waste utilization, the seeded precipitation was studied using synthesized sodium silicate solution containing different inorganic salt impurities. The results show that sodium chloride, sodium sulfate, sodium carbonate, or calcium chloride can change the siloxy group structure. The number of high-polymeric siloxy groups decreases with increasing sodium chloride or sodium sulfate concentration, which is detrimental to seeded precipitation. Calcium chloride favors the polymerization of silicate ions, and even the chain groups precipitate with the precipitation of high-polymeric sheet and cage-like siloxy groups. The introduced sodium cations in sodium carbonate render a more open network structure of high-polymeric siloxy groups, although the carbonate ions favor the polymerization of siloxy groups. No matter how the four impurities affect the siloxy group structure, the precipitates are always amorphous opal-A silica hydrate.

Key words: aluminosilicate; sodium silicate solution; siloxy group; impurity; silica hydrate

1 Introduction

To realize the comprehensive utilization of aluminosilicate solid wastes such as coal fly ash and coal gangue, we proposed a novel technique named as ferric oxide assisted roasting–alkali leaching silica–seeded precipitation [1]. In this technique, the aluminosilicate can be efficiently converted into aluminum concentrate, ferric oxide, and sodium silicate solution through the roasting–leaching process [2−4]. The resultant aluminum concentrate can be readily digested via the Bayer process to recover alumina, while the ferric oxide in the digestion residue can be recycled through roasting [5]. For recycling the alkaline leaching agent used in the leaching, seeded precipitation was proposed to extract silica from the resultant sodium silicate solution and some substantive progress has been achieved [1]. The precipitation rate of silica in the sodium silicate solution with a modulus of 3.0 can reach up to 72.17%, the spent solution modulus of 0.86 can be recycled to the leaching process of silica in the roasted product, and the granular opaline silica hydrate precipitated from solution can be widely used in industries [6] and agriculture [7]. Seeded precipitation could potentially contribute to realizing the waste-free cleaner utilization of aluminosilicate solid wastes, remarkably reducing the environmental pollution caused by the massive landfills where such wastes are dumped [8,9]. Moreover, during the precipitation, we found that the precipitation of silica hydrate is related to the siloxy group structure of sodium silicate solution, where the high-polymeric siloxy group determines the formation of silica hydrate. However, previous

Corresponding author: Qiu-sheng ZHOU, Tel/Fax: +86-731-88830453, E-mail: qszhou@csu.edu.cn
DOI: 10.1016/S1003-6326(24)66592-1

studies were limited to impurity-free sodium silicate solution. Real solution contains various impurities, such as calcium, iron, sulfur, carbon, chloride, and other impurity elements, which originate from aluminosilicate materials or leaching media, these impurities may enter into the solution during the alkali leaching of roasted products [10]. They may change the solution property and silicate species distribution, affecting the precipitation of the silicon products from sodium silicate solution.

Researchers have reported that the viscosity of sodium silicate solution increases with the introduction of sodium chloride, sodium sulfate, or sodium carbonate, and the effect of alkali chlorides (LiCl, NaCl and KCl) on the distribution of silicate species is manifested as a decrease in the content of monomeric or dimeric silicate species [11]. Additionally, some metal cations, such as calcium [12], aluminum [12], and iron [13], also affect the siloxy group structure. They induce the polymerization and flocculation of siloxy groups by shielding the surface charge of silicate ions [14] and are considered as silicate network modifiers. Alkali metal cations (e.g., sodium and potassium) control the formation of geopolymeric gels by affecting the distribution of silicate species in highly concentrated sodium silicate solution [15]. Unfortunately, to our best knowledge, there is no report about the effect of impurities such as sodium chloride, sodium sulfate, sodium carbonate and calcium chloride on both the distribution of high-polymeric siloxy groups and seeded precipitation, due to the structural complexity and behavioral specificity of sodium silicate solution. Therefore, based on our previous studies, the siloxy group distribution and seeded precipitation of silica hydrate from sodium silicate solution were systematically investigated in the presence of sodium chloride, sodium sulfate, sodium carbonate and calcium chloride with different concentrations. The improvement of this work may facilitate the efficient utilization of aluminosilicate solid wastes, reducing their environmental deterioration.

2 Experimental

2.1 Materials

In addition to industrial-grade sodium silicate (20.61 wt.% Na_2O, 60.03 wt.% SiO_2) procured from Qingdao Dongyue Sodium Silicate Co., Ltd., and active $SiO_2{\cdot}nH_2O$ seed obtained by the seeded precipitation from sodium silicate solutions using analytically pure $SiO_2{\cdot}nH_2O$ as seeds, all reagents used in this work were of analytically pure grades, including Na_2CO_3, Na_2SO_4, NaCl, $CaCl_2$, and $SiO_2{\cdot}nH_2O$ purchased from Sinopharm Chemical Reagent Co., Ltd., and NaOH from Xilong Science Co., Ltd., China.

2.2 Experimental procedure

The calculated and weighed industrial-grade sodium silicate and sodium hydroxide were dissolved with deionized water to synthesize sodium silicate solution with different concentrations, and inorganic sodium salts and calcium chloride impurities were added according to a concentration gradient of 0, 5, 15 g/L and 0, 1, 3 g/L, respectively. Sodium silicate solutions containing impurities were kept in a bath (DZKW-4, Beijing Yongguangming Medical Appliance Factory, China, ±0.5 °C) at 25 °C for 30 min and then analyzed via infrared spectrum using a solution coated on KBr with a scan number of 32 and a spectral resolution of 8 cm^{-1}.

Seeded precipitation experiments were carried out in a 500 mL beaker [1]. About 400 mL sodium silicate solution was put into the beaker placed in the bath preheated at 90 °C, followed by stirring and adding some $SiO_2{\cdot}nH_2O$ to raise the solution modulus. When the solution cooled down to the specified precipitation temperature, the inorganic salt impurity was introduced before adding a certain amount of analytically pure or active $SiO_2{\cdot}nH_2O$ seeds. After 12 h, about 10 mL of the slurry was taken out and then centrifuged to obtain a spent solution and a precipitation product. The treatment method for the precipitation product and the analysis methods of SiO_2, Na_2O concentration, and the precipitation rate η_t of silica are the same as those reported in our previous studies [1].

2.3 Characterization

The phase of the precipitation product was characterized via X-ray diffraction (Empyrean 2, Panalytical, Holland) with a Cu K_α radiation (λ=1.54 Å) at a scanning step of 0.01°. The structural spectra of the precipitation products were recorded using a Fourier transform infrared

spectrometer (Nicolet iS50, Thermo Fisher Scientific, USA) and a nuclear magnetic resonance spectrometer (Bruker Avance III HD 400, Bruker, Switzerland). Fourier transform infrared (FTIR) spectra were collected using a KBr disc technique with a spectral range of 400−4000 cm^{-1}, and the ^{29}Si nuclear magnetic resonance (NMR) single-pulse spectra were acquired using an operating frequency of 79.49 MHz and a spinning rate of 8 kHz. A recycle delay time of 5 s was used between each 90° pulse until 1600 scans were accumulated. The micromorphology and structure of the gel formed by the reaction of calcium chloride and sodium silicate solution were measured via transmission electron microscopy (TEM) by using a JEOL JEM−2100F analytical electron microscope (Japan Electronics Co., Ltd., Japan) with an accelerating voltage of 200 kV, a point resolution of 0.25 nm, a line resolution of 0.102 nm, and a scanning TEM resolution of 0.20 nm with a tilt angle (X/Y) of ±42°/±30°.

3 Results and discussion

3.1 Effect of inorganic salt impurities on siloxy group structure of sodium silicate solution

3.1.1 Sodium carbonate and sodium sulfate

To investigate the effect of sodium carbonate or sodium sulfate on the siloxy group of sodium silicate solution, FTIR spectral changes of the solutions were respectively studied at different concentrations of sodium carbonate or sodium sulfate impurity, as depicted in Fig. 1. The corresponding variations in the content of siloxy groups calculated using the method of spectral band area [16] are provided in Table 1. Apart from the water H—OH bending vibration of 1640 cm^{-1}, the water —OH stretching vibration of 3440 cm^{-1}, and the O—C—O asymmetric stretching vibration of 1412 cm^{-1}, four characteristic absorption peaks of Si—OH and Si—O bonds exist at 2017, 1025, 700 and 481 cm^{-1} in the infrared spectrum of sodium silicate solution. The Si — OH bond stretching vibration mode appears at 2017 cm^{-1}, and the Si — O — Si bond stretching vibration band characterizing the high-polymeric silicate species appears at 1025 cm^{-1} [17]. The Si—O bond bending vibration band representing the oligomeric silicate species appears at 700 and 481 cm^{-1} [18].

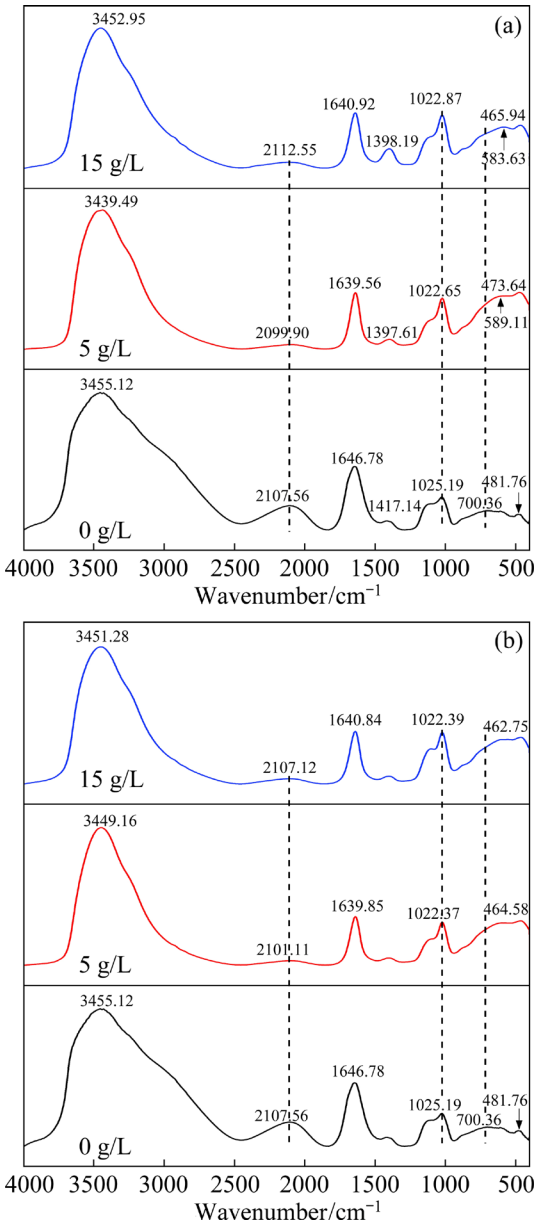

Fig. 1 FTIR spectra showing effect of Na_2CO_3 (a) or Na_2SO_4 (b) on structure of siloxy groups of sodium silicate solution ($\rho(Na_2O)$ 50.21 g/L; modulus 2.50)

Figure 1(a) shows that the introduction of sodium carbonate slightly reduces the absorption frequency of the Si—O—Si bond, which shifts from 1025 to 1022 cm^{-1}, indicating a more open network structure of high-polymeric siloxy groups and an increase in the bond distance between silicon and oxygen atoms [19]. This phenomenon is related to the fact that sodium ions with low hydration energy can replace some or most of the protons in the Helmholtz double electric layer [20]. The increased concentration of sodium cations in solution with the introduction of the impurity

leads to the breakage of the polymerized Si—O—Si bond [21]. Despite the red-shift of the absorption peak, the intensity of the Si—O—Si bond increases gradually, which is consistent with the result in Table 1 that the Si—O—Si bond content increases from 44.72% without impurities to 56.89% with 15 g/L sodium carbonate. The increase in the high-polymeric Si—O—Si bond content may be attributed to the action of carbonates, which promote the polymerization of silica [22]. The slightly higher absorption frequency for the Si—O—Si bond at 15 g/L Na_2CO_3 than that at 5 g/L Na_2CO_3 is precisely due to the combined effects of the destruction of sodium cation and the polymerization of carbonate anion. Meanwhile, the red-shift degree of the Si—O bond increases but its content decreases with increasing sodium carbonate concentration.

Table 1 Fraction of siloxy groups in solution at different impurity additions

Inorganic salt	Addition amount/(g·L^{-1})	Fraction of siloxy group/%		
		Si—OH	Si—O—Si	Si—O
−	0	33.58	44.72	21.70
Na_2CO_3	5	15.46	55.47	29.07
	15	18.63	56.89	24.48
Na_2SO_4	5	12.41	39.85	47.74
	15	12.55	44.38	43.07
NaCl	5	15.29	41.29	43.42
	15	22.76	34.36	42.88
$CaCl_2$	1	17.14	63.90	18.96
	3	26.07	68.00	5.93

$\rho(Na_2O)$ 50.21 g/L; modulus 2.50

When sodium sulfate impurity, a neutral salt, is added to the solution, the infrared spectral change is similar to that of the introduction of sodium carbonate impurity, that is, the absorption frequencies of the Si—O—Si and Si—O bonds shift towards a low-wavenumber due to the breakage effect of a large number of free sodium ions on the siloxy groups. However, the difference between the two impurities is that the Si—O bond bending vibration peak shifts towards the lower wavenumber in the presence of sodium sulfate impurity, i.e., from 700 cm^{-1} to a low absorption frequency of 462 cm^{-1}. The possible reason is as follows: not only can the sodium cation in sodium sulfate break the polymerization of the siloxy groups, but the negatively charged sulfate ions also repel the homoelectric silicate ion, hindering the condensation of siloxy group [23].

3.1.2 Sodium chloride and calcium chloride

The properties of the zeta potential, activity, and colloidal stability of sodium silicate solutions including sodium chloride or calcium chloride have been reported in the literature [24], along with the solubility variation of amorphous silica in two salt solutions [25]. However, the relationship between the two salts and the siloxy group structure is indistinct due to the complex and variable solution structure. Experiments were conducted by adding sodium chloride of 5 and 15 g/L or calcium chloride of 1 and 3 g/L. Figure 2(a) indicates that sodium chloride reduces the polymerization degree of silicate ions. With increasing sodium chloride concentration, the peak position of the high-polymeric Si—O—Si bond shifts from 1025 to 1023 cm^{-1}, the intensity of the Si—O bond peak increases as the peak position shifts towards low-wavenumber, and the content of the Si—O bond increases from 21.70% without impurities to about 43.00% with impurities (Table 1). Meanwhile, Table 1 indicates that the content of the Si—O—Si bond characterizing high-polymeric silicate species progressively decreases with increasing sodium chloride concentration. This phenomenon can be explained by the increased substitution of bridging oxygens in polymeric silicate ions by non-bridging oxygens under the enhanced destructive effect of the sodium ion. The increase in the Si—O bond content and the decrease in the Si—O—Si bond content manifest that sodium chloride inhibits the polymerization of siloxy groups.

When the sodium cation in sodium chloride impurity is replaced with calcium ion, the intensity and red-shift degree of the stretching vibration peak of siloxy groups increase, because the calcium cation can promote the polymerization of silicate ions, resulting in the condensation of the high-polymeric siloxy group to precipitate silica gel [26], and decreasing the absorption frequencies of silicate ions in solution. In this experiment, the flocculent gel did appear in the region where calcium chloride was added. This result is significantly different from the introduction of other inorganic sodium salt impurities. The conclusion that calcium ions can

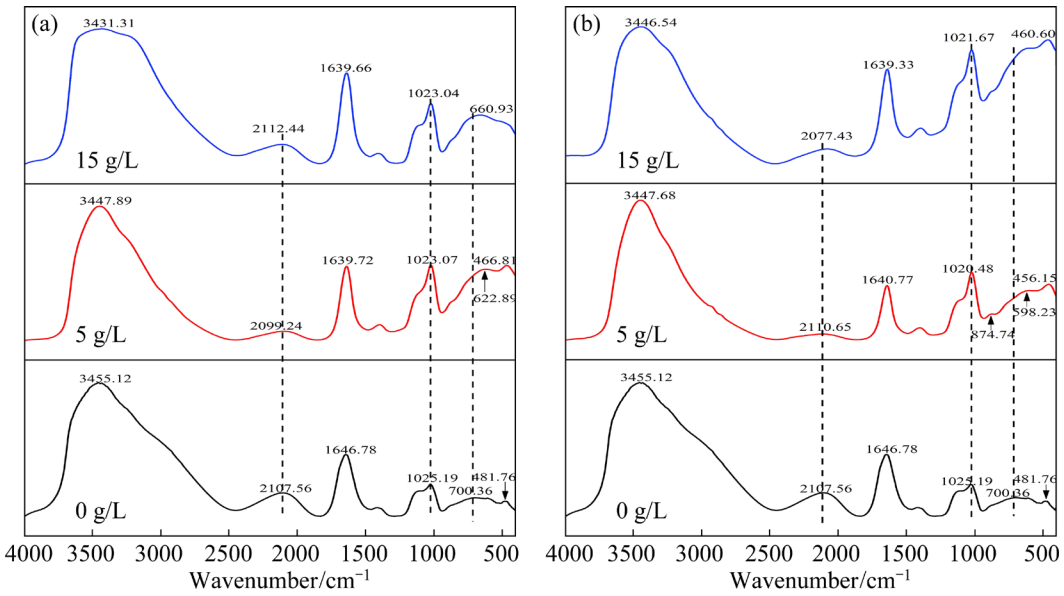

Fig. 2 FTIR spectra showing effect of NaCl (a) or $CaCl_2$ (b) on siloxy group structure of sodium silicate solution ($\rho(Na_2O)$ 50.21 g/L; modulus 2.50)

promote the polymerization of silicate is also confirmed by the variation laws of a sharp increase in Si—O—Si bond content and a significant decrease in Si—O bond content in the presence of calcium chloride in Table 1. That is, the Si—O—Si bond content increases sequentially from 44.72% (0 g/L $CaCl_2$) to 63.90% (1 g/L $CaCl_2$) and 68.00% (3 g/L $CaCl_2$) while the Si—O bond content decreases orderly from 21.70% (0 g/L $CaCl_2$) to 18.96 % (1 g/L $CaCl_2$) and 5.93% (3 g/L $CaCl_2$). Additionally, new silicate species occur at 874 cm^{-1} in the infrared spectrum of the sodium silicate solution containing 1 g/L $CaCl_2$, implying that the process of the calcium cation promoting the polymerization and precipitation of silicate will make the siloxy group structure more complex.

3.2 Effect of inorganic salt impurities on seeded precipitation of silica hydrate from sodium silicate solution

The distribution and polymerization degree of silicate species in solution determine the seeded precipitation of silica hydrate from sodium silicate solution. The structural changes of the siloxy groups caused by inorganic salt impurities, such as NaCl, Na_2SO_4, Na_2CO_3 and $CaCl_2$, could directly affect the seeded precipitation. For this reason, the seeded precipitation from sodium silicate solutions with a modulus of 2.50 [3] and various inorganic salt impurities was investigated by using a temperature-drop program under the conditions of 40.48 g/L Na_2O of the pregnant silicate solution and 280 g/L liquor active seed amount. The influence behavior of impurities was reflected by the variations in precipitation rate of silica and the structure of precipitation product obtained from the solution.

3.2.1 Preparation and characterization of active seed

The active seed was prepared in a sodium silicate solution with a modulus of 2.5 and 50.21 g/L Na_2O using analytically pure $SiO_2{\cdot}nH_2O$ (the original seed) as seed under the conditions of 400 g/L liquor seed at 50 °C for 17 h. The XRD, FTIR and ^{29}Si NMR spectra of the active seed (precipitation product) are shown in Fig. 3. A single broad peak exists at 2θ value between 16° and 35° (maximum intensity centered at 2θ=22.5°) in the XRD patterns of original seed and precipitation product, signifying that they are amorphous. Such diffraction spectrum characterizing active seed could be classified as opal-A [27]. Figures 3(b, b′) show that there are four distinct silicate characteristic absorption peaks in the infrared spectrum of original seed, apart from the characteristic absorption bands of water (3453.32 and 1639.40 cm^{-1}). These peaks appear at 1085.28, 960.99, 797.62 and 465.99 cm^{-1}, and represent Si—O—Si bond antisymmetric stretching vibration,

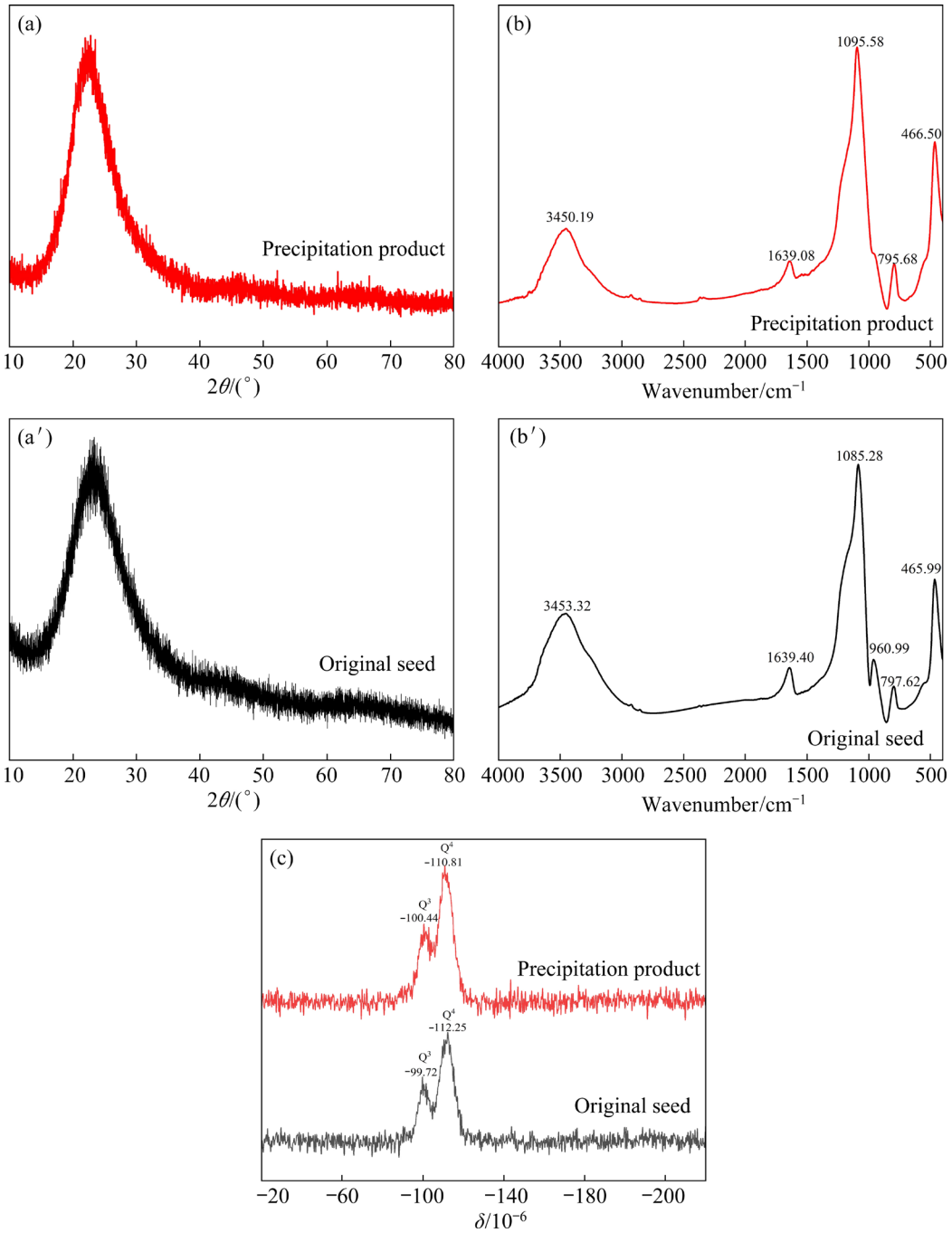

Fig. 3 XRD (a, a′), FTIR (b, b′) and ^{29}Si NMR (c) spectra of original seed and precipitation product (ρ(Na_2O) 50.21 g/L; modulus 2.50; seed amount 400 g/L; temperature 50 °C; duration 17 h)

Si—OH bond bending vibration, Si—O—Si bond symmetric stretching vibration, and Si—O bond bending vibration, respectively. Compared with original seed, the Si—OH bond bending vibration band disappears for precipitation product, implying that the internal silanol groups also polymerize to transform eventually into siloxane bonds during the precipitation of the product [28], exhibiting a higher absorption frequency of the high-polymeric Si—O—Si bond in precipitation product than that in original seed. Meanwhile, the disappearance of the Si—OH bond also reflects that the water content in product is lower than that in original seed [29]. Whether the solid sample is an original seed or a precipitation product, two chemical shift points can be observed in their ^{29}Si NMR spectra. One is located around -99.92×10^{-6} and the other is found near -12.25×10^{-6}, representing sheet and

cage-like siloxy groups with increasing polymerization degree, respectively, which is in agreement with the findings reported in the literature for the amorphous opal NMR spectrum [30]. Combining the phase, infrared structure analysis with the ^{29}Si NMR result of precipitation product, the product precipitated from sodium silicate solution is opal-A silica hydrate ($SiO_2 \cdot nH_2O$) polymerized by the high-polymeric siloxy groups.

3.2.2 Effect of inorganic salt impurities on precipitation rate of silica

The precipitation rate (η_t) of silica can directly estimate the effectiveness of the seeded precipitation. The effects of inorganic sodium salts (sodium carbonate, sodium sulfate, and sodium chloride) and calcium chloride impurities on precipitation rate of silica and solution modulus during the seeded precipitation are plotted in Fig. 4 and listed in Table 2. The data in the figure and the table are the average of three repeated experiments.

The results from Fig. 4(a) indicate that sodium carbonate is conducive to precipitating the silica product. The η_t of silica for the solution with sodium carbonate impurity is higher than that for the solution without impurity during the same precipitation duration, and the promoting effect increases with increasing sodium carbonate concentration. With the continuous precipitation of silica product, the solution modulus gradually decreases. As indicated in Table 2, the solution modulus at 15 g/L sodium carbonate is 0.87 for 48 h, which is markedly lower than that of the solution without impurity. When the anion in the inorganic sodium salt impurity is chloride or sulfate ion, the η_t of silica decreases and the solution modulus increases, proclaiming that both sodium chloride and sodium sulfate restrain the seeded precipitation.

Compared with inorganic sodium salts, the effect of calcium chloride on the seeded precipitation is much more complex. The content of high-polymeric siloxy groups in solution becomes lower

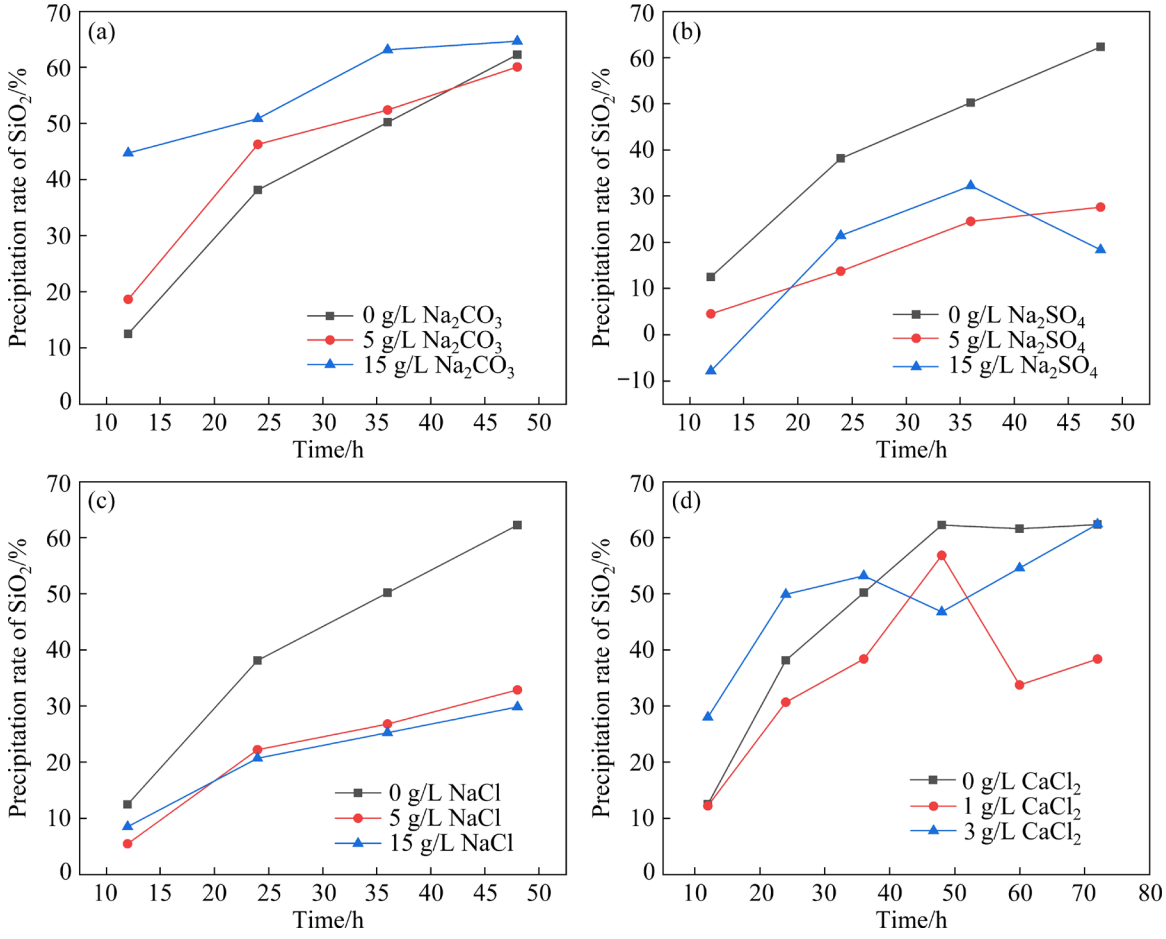

Fig. 4 Effect of Na_2CO_3 (a), Na_2SO_4 (b), NaCl (c) or $CaCl_2$ (d) on seeded precipitation from sodium silicate solution (Pregnant sodium silicate solution: $\rho(Na_2O)$ 40.48 g/L, modulus 2.50; seed amount 280 g/L; Temperature regime 1: initial temperature 45 °C, $t \leq 12$ h; Temperature regime 2: terminal temperature 40 °C, $t > 12$ h)

Table 2 Effect of inorganic salt impurities on solution modulus after precipitation duration (M_t)

Inorganic salt	Addition amount/ ($g \cdot L^{-1}$)	M_t					
		12 h	24 h	36 h	48 h	60 h	72 h
−	0	2.20	1.55	1.25	0.95	0.94	0.94
Na_2CO_3	5	2.01	1.33	1.18	0.99	−	−
	15	1.37	1.22	0.91	0.87	−	−
Na_2SO_4	5	2.37	2.29	1.87	1.79	−	−
	15	2.67	1.95	1.68	2.02	−	−
NaCl	5	2.39	1.96	1.85	1.69	−	−
	15	2.31	2.00	1.89	1.77	−	−
$CaCl_2$	1	2.20	1.74	1.55	1.08	1.66	1.55
	3	1.78	1.24	1.16	1.32	1.12	0.93

(Pregnant sodium silicate solution: $\rho(Na_2O)$ 40.48 g/L, modulus 2.50; seed amount 280 g/L; Temperature regime 1: initial temperature 45 °C, $t \leq 12$ h; Temperature regime 2: terminal temperature 40 °C, $t > 12$ h)

due to the precipitation of some high-polymeric siloxy groups preferentially forming flocculent gel during the introduction of calcium chloride, leading to a low precipitation rate of silica at a low calcium chloride concentration. Increasing calcium chloride concentration to 3 g/L, the reaction rate of seeded precipitation accelerates in the initial stage. Nonetheless, the η_t values of silica and the solution modulus for 3 g/L calcium chloride are close to the results for 0 g/L calcium chloride in the late stage. From Fig. 4(d), an extraordinary phenomenon was observed within the range of 36−48 h with 3 g/L $CaCl_2$ or 48−60 h with 1 g/L $CaCl_2$, both η_t of SiO_2 diminish, which might be ascribed to the rapid dissolution of some fine particles because of the relatively low supersaturation. We also noted that the existence of calcium chloride prolongs the precipitation period of sodium silicate solution compared with inorganic sodium salts. The adsorption and complexation between silicate and calcium ions enable the precipitation product to precipitate preferentially in the form of gel [31], decreasing the amount of high-polymeric siloxy groups in the system which form granular products and the probability of collision polycondensation between silicate ions, making the seeded precipitation from sodium silicate solution containing calcium chloride impurity longer.

The higher concentration of silica in sodium silicate solution means a greater polymerization degree of the silicate and a higher number of high-polymeric siloxy groups [32], which is more favorable for the seeded precipitation. Combined with the structural evolution of siloxy group of sodium silicate solution in the existence of inorganic salts, it can be assumed that the transformation of high-polymeric silicates to an oligomeric structure by either Na_2SO_4 or NaCl and the polymerization of silicate ions promoted by either carbonate anion in Na_2CO_3 or calcium cation in $CaCl_2$ are the major reasons affecting the seeded precipitation from sodium silicate solution.

Given the appearance of flocculent gel during the addition of calcium chloride into sodium silicate solution, the phase, structure, and morphology of this gel are investigated to identify whether it is silica hydrate or calcium silicate, as shown in Figs. 5 and 6. The diffraction pattern of the gel basically coincides with that of the precipitation product but differs significantly from the characteristic spectrum of the amorphous calcium silicate gel marked by a large diffuse diffraction peak centered at 30° (2θ) [18]. This result suggests that the gel precipitate from the solution may be an amorphous silica hydrate. The FTIR spectrum of the gel reveals the structural inheritance with opal-A silica hydrate, confirming the possibility that the gel is an opaline silica hydrate. The weak absorption peak of the CO_3^{2-} antisymmetric stretching vibration band near 1470 cm^{-1} in the spectrum can be attributed to the action of calcium during the formation of gel [33]. The morphologies of the gel in Figs. 6(a_1−a_4) show that the lamellar gel is composed of small subspherical particles agglomerated and stacked on top of one another, and this result is coincident with the morphology of the lamellar opal-A reported in the literature [34]. The element distribution in the gel mapping Figs. 6(b_1−b_6) display that calcium atoms are embedded around the siloxy groups composed of silicon and oxygen atoms, and their content accounts for about 5.45% of the total amount of all elements, while sodium content is lower, only 0.43%. The diversity in the content of two atoms is similar to the substitution of sodium atoms by high-valence calcium atoms during the formation of layered clay minerals [35]. Calcium atoms preferentially coordinate with the siloxy groups and are distributed

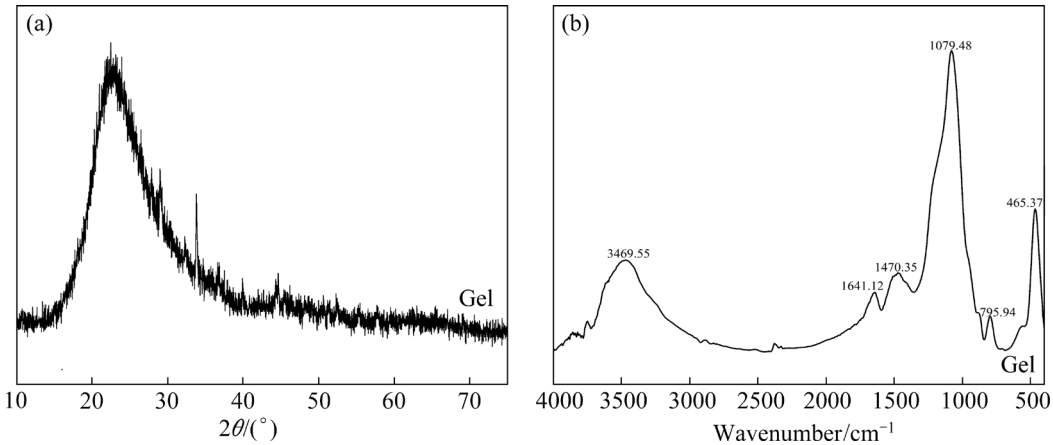

Fig. 5 XRD pattern (a) and FTIR spectrum (b) of gel formed in calcium chloride impurity system

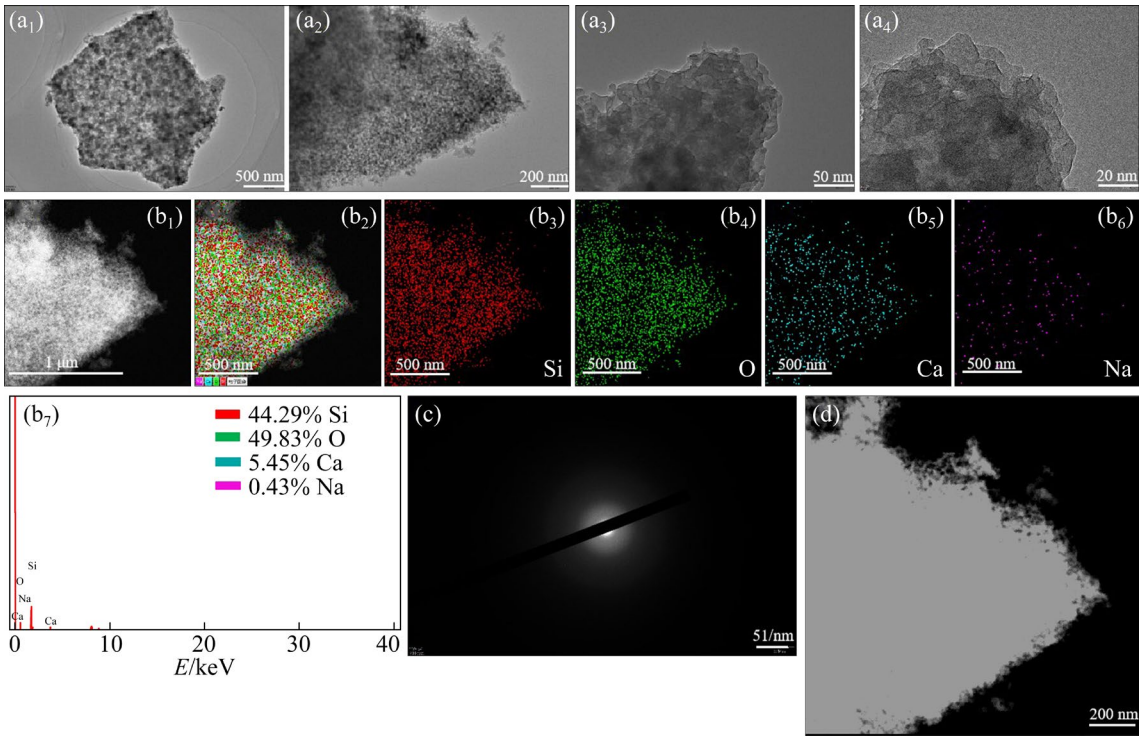

Fig. 6 TEM morphology (a_1−a_4), mappings and corresponding atom content (b_1−b_7), SAED pattern (c), and STEM (HAADF) (d) of gel

in the interstitial site of the silicate network [36]. The selected area electron diffraction (SAED) pattern of the gel has only one diffuse central spot and no neat crystal lattice pattern appears, indicating that the structure of the gel is amorphous. From Fig. 6(d), no crystalline phase and short-range ordered structural units occur in the gel, further testifying that the flocculent gel structure is non-crystalline. Based on the aforementioned results of the phase, infrared spectrum, and TEM analyses, the gel can be confirmed as an amorphous silica hydrate rather than calcium silicate.

3.2.3 Structural evolution of precipitation product in the presence of inorganic salt impurities

The connectivity of silicate species in the solution governs the polymerization degree of the solid [37], and the variation in the silicate polymerization degree of the solid feeds back the seeded precipitation effectiveness of sodium silicate solution. To clarify the effect of inorganic salt impurities on seeded precipitation, the structures of precipitation products precipitated from sodium silicate solution were studied under the conditions of adding 15 g/L inorganic sodium salts or 3 g/L

calcium chloride. The XRD patterns in Fig. 7(a) show that four precipitation products are of long-range disordered amorphous structure, and their diffraction peak shapes and characteristic diffraction positions are consistent with the diffraction pattern of active seed, demonstrating that inorganic sodium salts and calcium chloride exert minimal influence on the crystal morphology of the product. The FTIR spectra of precipitation products exhibit that the product structure inherited the active seed structure regardless of whether the impurities introduced into the solution were sodium carbonate, sodium sulfate, sodium chloride, or calcium chloride. The characteristic peaks of siloxy groups appearing near 1094, 795 and 467 cm^{-1} illustrate that inorganic salt impurities nearly have no effect on the molecular configuration of precipitation product. By the XRD and FTIR results in Fig. 7, the precipitation products obtained from the solutions with various impurities can be inferred as opal-A silica hydrate.

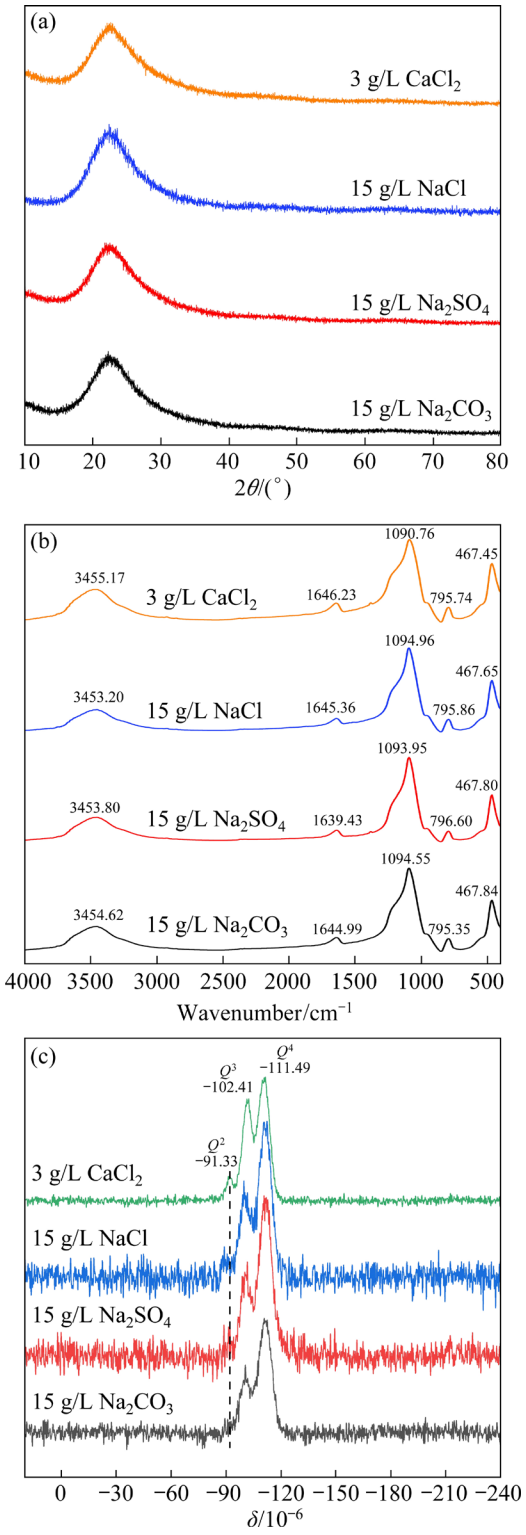

Fig. 7 XRD patterns (a), FTIR spectra (b) and ^{29}Si NMR (c) spectra of precipitation products in the presence of different impurities

From the macro perspective, XRD pattern provides the structural information of the long-range disorder of the product, and the FTIR spectrum has clarified the internal structural relationship between silicon and oxygen atoms from the microscopic perspective. Nevertheless, the internal structural information of the product can be more clearly displayed by solid-state high-resolution NMR spectroscopy. The ^{29}Si NMR spectra of precipitation products obtained from the solutions with inorganic salt impurities were recorded and the results are given in Fig. 7(c) and Table 3. The peak shapes of the ^{29}Si NMR spectra of precipitation products in the three inorganic sodium salt systems are the same as those of the added seeds. The spectra reveal a small shoulder at -102.41×10^{-6} in addition to the primary peak, which is centered at about -111.49×10^{-6}, demonstrating that the product precipitated from sodium silicate solution comprising inorganic sodium salt impurity is also amorphous silica hydrate [30]. Apart from the primary resonance peaks of cage-like (Q^4) and sheet (Q^3) siloxy groups, a weak peak of chain siloxy groups [38] is also found at -91.33×10^{-6} in the ^{29}Si NMR spectrum of the precipitation product for 3 g/L calcium chloride. The appearance of the -91.33×10^{-6} resonance peak may be explained by the strong adsorption and complexation effect between calcium cation and silicate anion [31]. The full width at half maximum (FWHM) values of the Q^4 resonance peak for four precipitation products all lie within the range of the FWHM value for the opal-A silica hydrate [39], although they are larger than 7.83×10^{-6} of the active

Table 3 ^{29}Si chemical shifts and full width at half maximum (FWHM) in precipitation product with different impurity systems

Sample	Inorganic salt	Addition amount/ ($g \cdot L^{-1}$)	Chemical shift/10^{-6}			FWHM/ 10^{-6}
			Q^2	Q^3	Q^4	
Activated seed	–	–	–	–100.44	–110.81	7.83
Precipitation product	Na_2CO_3	15	–	–101.55	–110.87	8.77
Precipitation product	Na_2SO_4	15	–	–101.62	–110.79	8.43
Precipitation product	NaCl	15	–	–99.77	–112.43	8.21
Precipitation product	$CaCl_2$	3	–91.33	–102.41	–111.49	9.15

seed in Table 3. Therefore, the precipitation products are all amorphous opal-A silica hydrate regardless of the presence of inorganic salt impurities during the seeded precipitation.

4 Conclusions

(1) Sodium sulfate or sodium chloride can restrain the polymerization of siloxy groups and seeded precipitation of silica hydrate from sodium silicate solution, while carbonate anions in sodium carbonate improve the precipitation rate of silica, but the structure of high-polymeric siloxy groups is more open due to the introduction of excessive sodium cations.

(2) The polymerization degree of siloxy groups in sodium silicate solution increases with elevated calcium chloride concentration. The rapid precipitation of the high-polymeric siloxy groups into gel in the initial stage prolongs the precipitation period and is detrimental to the precipitation of crystalline silica hydrate. The chain siloxy groups precipitate into product along with the high-polymeric sheet and cage-like siloxy groups under the action of calcium chloride.

(3) The gel formed during the addition of calcium chloride into sodium silicate solution is an amorphous silica hydrate rather than calcium silicate. However, some calcium atoms are distributed in the interstitial site of the silicate network during gel formation.

(4) Inorganic salt impurity does not affect the molecular configuration of precipitation product. Whether the impurities introduced into sodium silicate solution are inorganic sodium salts or calcium chloride, the precipitation products are all amorphous opal-A silica hydrate.

CRediT authorship contribution statement

Xiao-bin LI: Conceptualization, Supervisor, Methodology, Review; **Xiao-bing GAO:** Investigation, Data curation, Validation, Writing − Original draft; **Qiu-sheng ZHOU:** Supervisor, Writing − Review & editing; **Yi-lin WANG**, **Tian-gui QI**, **Lei-ting SHEN**, **Gui-hua LIU**, and **Zhi-hong PENG:** Resources.

Declaration of competing interest

The authors declare that they have no known competing financial interests or personal relationships that could have appeared to influence the work reported in this paper.

Acknowledgments

The authors are grateful for the financial support from the National Natural Science Foundation of China (No. 52074364).

References

[1] LI Xiao-bin, GAO Xiao-bing, WANG Yi-lin, ZHOU Qiu-sheng, LIU Gui-hua, PENG Zhi-hong, QI Tian-gui. Coal fly ash cleaner utilization by ferric oxide assisted roasting – leaching silica: Recycling lixiviant by seeded precipitation of leachate [J]. Process Safety and Environmental Protection, 2022, 164: 827−835.

[2] LI Xiao-bin, WANG Peng, WANG Hong-yang, ZHOU Qiu-sheng, QI Tian-gui, LIU Gui-hua, PENG Zhi-hong, WANG Yi-lin, SHEN Lei-ting. The alkaline leaching behavior of silica solid solutions in the product obtained by roasting the mixture of high-alumina coal gangue and hematite [J]. Journal of Sustainable Metallurgy, 2022, 8: 1853−1865.

[3] HUANG Qing-ping, ZHOU Qiu-sheng, LI Xiao-bin, QI Tian-gui, PENG Zhi-hong, LIU Gui-hua. Dynamic expansion experiment of efficient separation of aluminum and silicon from coal fly ash [J]. The Chinese Journal of Nonferrous Metals, 2022, 32: 173−182. (in Chinese)

[4] WANG Hong-yang, ZHANG Xiao-xue, YANG Si-yuan, LIU Cheng, LUO Li-qun. Separation of alumina and silica from metakaolinite by reduction roasting-alkaline leaching process: Effect of $CaSO_4$ and CaO [J]. Transactions of Nonferrous Metals Society of China, 2022, 32: 999−1009.

[5] LI Xiao-bin, WANG Hong-yang, ZHOU Qiu-sheng, QI Tian-gui, LIU Gui-hua, PENG Zhi-hong. Efficient separation of silica and alumina in simulated CFB slag by reduction roasting-alkaline leaching process [J]. Waste Management, 2019, 87: 798−804.

[6] WU Zong-shan, XIE Jing-jing, LIU Hai-bo, CHEN Tian-hu, CHENG Peng, WANG Can, KONG Dian-chao. Preparation, characterization, and performance of 4A zeolite based on opal waste rock for removal of ammonium ion [J]. Adsorption Science & Technology, 2018, 36: 1700−1715.

[7] CLARKE J. The occurrence and significance of biogenic opal in the regolith [J]. Earth-Science Reviews, 2003, 60: 175−194.

[8] ZHU Li, JI Jia-you, WANG Shu-lin, XU Chen-xi, YANG Kun, XU Man. Removal of Pb(II) from wastewater using Al_2O_3−NaA zeolite composite hollow fiber membranes synthesized from solid waste coal fly ash [J]. Chemosphere, 2018, 206: 278−284.

[9] ZHANG Yu-juan, SUN Jun-min, LÜ Guo-zhi, ZHANG Ting-an, GONG Yan-bing. Kinetics of alumina extraction from coal gangue by hydrochloric acid leaching [J]. Transactions of Nonferrous Metals Society of China, 2023, 33: 1932−1942.

[10] QI Fang, ZHU Gan-yu, ZHANG Yi-min, HOU Xin-juan, LI Shao-peng, YANG Chen-nian, ZHANG Jian-bo, LI Hui-quan. Eco-utilization of silicon-rich lye: Synthesis of amorphous calcium silicate hydrate and its application for recovering heavy metals [J]. Separation and Purification Technology, 2022, 282: 120092−120103.

[11] DUTTA P K, SHIEH D C. Influence of alkali chlorides on distribution of aqueous base solubilized silicate species [J]. Zeolites, 1985, 5: 135−138.

[12] FENG Yan, CHEN Qiu-song, ZHOU Yan-long, YANG Qi-xing, ZHANG Qin-li, JIANG Liang, GUO Hong-quan. Modification of glass structure via CaO addition in granulated copper slag to enhance its pozzolanic activity [J]. Construction and Building Materials, 2020, 240: 117970−117979.

[13] WEIGEL C, CORMIER L, CALAS G, GALOISY L, BOWRON D T. Intermediate-range order in the silicate network glasses $NaFe_xAl_{1-x}Si_2O_6$ (x=0, 0.5, 0.8, 1): A neutron diffraction and empirical potential structure refinement modeling investigation [J]. Physical Review B, 2008, 78: 064202-1−064202-11.

[14] LOPEZ P J, GAUTIER C, LIVAGE J, CORADIN T. Mimicking biogenic silica nanostructures formation [J]. Current Nanoscience, 2005, 1: 73−83.

[15] PROVIS J L, DUXSON P, LUKEY G C, SEPAROVIC F, KRIVEN W M, van DEVENTER J S J. Modeling speciation in highly concentrated alkaline silicate solutions [J]. Industrial & Engineering Chemistry Research, 2005, 44: 8899−8908.

[16] LI Xiao-bin, WANG Dan-qin, ZHOU Qiu-sheng, LIU Gui-hua, PENG Zhi-hong. Concentration variation of aluminate ions during the seeded precipitation process of gibbsite from sodium aluminate solution [J]. Hydrometallurgy, 2011, 106: 93−98.

[17] DIMAS D, GIANNOPOULOU I, PANIAS D. Polymerization in sodium silicate solutions: A fundamental process in geopolymerization technology [J]. Journal of Materials Science, 2009, 44: 3719−3730.

[18] LECOMTE I, HENRIST C, LIÉGEOIS M, MASERI F, RULMONT A, CLOOTS R. (Micro)-structural comparison between geopolymers, alkali-activated slag cement and Portland cement [J]. Journal of the European Ceramic Society, 2006, 26: 3789−3797.

[19] ZHU Hui, MA Yu-guang, FAN Yu-guo, SHEN Jia-cong. Fourier transform infrared spectroscopy and oxygen luminescence probing combined study of modified sol−gel derived film [J]. Thin Solid Films, 2001, 397: 95−101.

[20] ZHOU Zhong-shi, LI Chun-sheng, JIN Jian-zhong, HE Xue-han. Effect of sodium chloride on gelatinization of silicic acid and the formation of novel polysilicic acid crystals [J]. Journal of Non-Crystalline Solids, 2007, 353: 2774−2778.

[21] PALOMO A, DELA FUENTE J I L. Alkali-activated cementitous materials: Alternative matrices for the immobilisation of hazardous wastes: Part I. Stabilisation of boron [J]. Cement and Concrete Research, 2003, 33: 281−288.

[22] KOO T, LEE Y J, SHEIKHOLESLAMI R. Silica fouling and cleaning of reverse osmosis membranes [J]. Desalination, 2001, 139: 43−56.

[23] CRIADO M, JIMÉNEZ A F, PALOMO A. Effect of sodium sulfate on the alkali activation of fly ash [J]. Cement and Concrete Composites, 2010, 32: 589−594.

[24] HUANG Wei-an, LAN Qiang, QIU Zheng-song, ZHANG Yan, ZHONG Han-yi, FENG Guang-tong. Colloidal properties and clay inhibition of sodium silicate in solution and montmorillonite suspension [J]. Silicon, 2016, 8: 111−122.

[25] MARSHALL W L, WARAKOMSKI J M. Amorphous silica solubilities II. Effect of aqueous salt solutions at 25 °C [J]. Geochimica et Cosmochimica Acta, 1980, 44: 915−924.

[26] KUZENTSOVA T F. Effect of calcium cation on the structure of silica gel formed from decationized sol [J]. Russian Journal of Applied Chemistry, 2001, 74: 855−859.

[27] SPRYNSKYY M, POMASTOWSKI P, HORNOWSKA M, KRÓL A, RAFIŃSKA K, BUSZEWSKI B. Naturally organic functionalized 3D biosilica from diatom microalgae [J]. Materials & Design, 2017, 132: 22−29.

[28] LOUCAIDES S, BEHRENDS T, VAN CAPPELLEN P. Reactivity of biogenic silica: Surface versus bulk charge density [J]. Geochimica et Cosmochimica Acta, 2010, 74: 517−530.

[29] AWADH S M, YASEEN Z M. Investigation of silica polymorphs stratified in siliceous geode using FTIR and XRD methods [J]. Materials Chemistry and Physics, 2019, 228: 45−50.

[30] ADAMS S J, HAWKES G E, CURZON E H. A solid state ^{29}Si nuclear magnetic resonance study of opal and other hydrous silicas [J]. American Mineralogist, 1991, 76: 1863−1871.

[31] TANG Shan-yu, YANG Cheng-zhi. Studies on interaction between sodium silicates and calcium ions [J]. Oilfield Chemistry, 1989, 6: 147−151. (in Chinese)

[32] ALVAREZ R, SPARKS D L. Polymerization of silicate

anions in solutions at low concentrations [J]. Nature, 1985, 318: 649−651.
[33] SOLONENKO A P, BLESMAN A I, POLONYANKIN D A, BEL'SKAYA L V. Peculiarities of the composition of solid phases formed in aqueous calcium−silicate systems with a medium of variable acidity [J]. Glass Physics and Chemistry, 2017, 43: 452−458.
[34] ELSASS F, DUBROEUCQ D, THIRY M. Diagenesis of silica minerals from clay minerals in volcanic soils of Mexico [J]. Clay Minerals, 2000, 35: 477−489.
[35] SUTER J L, COVENEY P V, ANDERSON R L, GREENWELL H C, CLIFFE S. Rule based design of clay-swelling inhibitors [J]. Energy & Environmental Science, 2011, 4: 4572−4586.
[36] ALLALI F, JOUSSEIN E, KANDRI N I, ROSSIGNOL S. The influence of calcium content on the mixture of sodium silicate with different additives: Na_2CO_3, NaOH and AlO(OH) [J]. Construction and Building Materials, 2016, 121: 588−598.
[37] NIETO P, ZANNI H. Polymerization of alkaline−calcium−silicate hydrates obtained by interaction between alkali-silica solutions and calcium compounds. A ^{29}Si nuclear magnetic resonance study [J]. Journal of Materials Science, 1997, 32: 3419−3425.
[38] BROWN L D, RAY A S, THOMAS P S. ^{29}Si and ^{27}Al NMR study of amorphous and paracrystalline opals from Australia [J]. Journal of Non-Crystalline Solids, 2003, 332: 242−248.
[39] de JONG B H W S, van HOEK J, VEEMAN W S, MANSON D V. X-ray diffraction and ^{29}Si magic-angle-spinning NMR of opals: Incoherent long- and short-range order in opal-CT [J]. American Mineralogist, 1987, 72: 1195−1203.

无机盐杂质对硅酸钠溶液晶种分解析出二氧化硅水合物的影响

李小斌，高小兵，周秋生，王一霖，齐天贵，申雷霆，刘桂华，彭志宏

中南大学 冶金与环境学院，长沙 410083

摘　要：为明确真实铝硅酸盐固体废物脱硅液通过添加晶种析出水合二氧化硅的情况和提高固废综合利用率，利用含有不同无机盐杂质的合成硅酸钠溶液进行晶种分解研究。结果表明：氯化钠、硫酸钠、碳酸钠或氯化钙能改变硅氧基团的结构。高聚合态硅氧基团数量随氯化钠或硫酸钠浓度的增加而减少，对晶种分解不利。氯化钙有利于硅酸盐离子聚合，链状硅氧基团甚至会伴随着高聚合态层状和网状基团的析出而析出。碳酸钠中碳酸根离子也有利于硅氧基团聚合，但引入的钠阳离子使高聚合态硅氧基团网状结构更加开放。不管这四种杂质如何影响溶液中硅氧基团结构，析出产物均为无定形蛋白石-A 型二氧化硅水合物。

关键词：铝硅酸盐；硅酸钠溶液；硅氧基团；杂质；二氧化硅水合物

(Edited by Xiang-qun LI)